Transport in Porous Media **42:** 133–154, 2001.

Macrodispersivity and Large-scale Hydrogeologic Variability

DENNIS McLAUGHLIN[1] and FENG RUAN[2]
[1]*Ralph M. Parsons Laboratory, Department of Civil and Environmental Engineering, Massachusetts Institute of Technology, Cambridge, MA 02139, U.S.A.*
[2]*Applications Research, Schlumberger GeoQuest, Houston, TX 77056, U.S.A.*

(Received: 16 March 1999; in final form: 21 December 1999)

Abstract. Although groundwater velocities vary over a wide range of spatial scales it is generally only feasible to model the largest variations explicitly. Smaller-scale velocity variability must be accounted for indirectly, usually by increasing the magnitude of the dispersivity tensor (i.e. by introducing a so-called macrodispersivity). Most macrodispersion theories tacitly assume that a macrodispersivity tensor which works well when there is only small-scale velocity variability will also work well when there is larger-scale variability. We analyze this assumption in a high resolution numerical experiment which simulates solute transport through a two-scale velocity field. Our results confirm that a transport model which uses an appropriately adjusted macrodispersivity can reproduce the large-scale features of a solute plume when the velocity varies only over small scales. However, if the velocity field includes both small and large-scale components, the macrodispersivity term does not appear to be able to capture all of the effects of small-scale variability. In this case the predicted plume is more well mixed and consistently underestimates peak solute concentrations at all times. We believe that this result can be best explained by scale interactions resulting from the nonlinear transformation from velocity to concentration. However, additional analysis will be required to test this hypothesis.

Key words: macrodispersion, multi-scale, solute transport.

1. Introduction

It is now widely acknowledged that the hydrogeological properties which control solute transport in the subsurface vary over a wide range of space and/or time scales. In practical modeling studies it is convenient to make a fundamental distinction between large-scale variability that can be measured or inferred from site-specific information and smaller-scale variability that cannot be resolved. Unresolved fluctuations in hydraulic conductivity, recharge, and other quantities may have significant, but difficult to predict, effects on larger-scale solute transport. The resulting uncertainty can be accounted for explicitly with a stochastic description of solute transport which seeks to predict probability distributions, or at least ensemble moments, of the solute concentration.

Much attention has been devoted in recent years to the development of theories that predict the statistical properties of solute plumes transported through velocity

fields characterized by small-scale variations about a known constant mean (Gelhar and Axness, 1983; Gelhar, 1986; Dagan, 1984, 1986, 1989, 1990; Neuman *et al.*, 1987). Many of these studies have focused on derivations of the ensemble mean of the solute concentration. The hope is that this mean will provide useful information about the behavior, not only of a hypothetical ensemble, but also of particular real-world plumes. Of course, we don't expect any specific plume to look exactly like the ensemble mean. But it would be useful if the ensemble mean correctly predicted important large-scale features of the plume, such as its spatial moments or the percentage of plume area with concentrations exceeding a given threshold.

Efforts to investigate connections between the ensemble mean concentration and the properties of particular plumes have tended to focus on the first two spatial moments of concentration. These moments provide convenient quantitative measures of the translation and spreading of particular plumes. The basis for a probabilistic description of solute variability is a hypothetical ensemble (or population) of solute plumes. This ensemble is characterized by a set of probability densities which define the first, second, ... nth-order statistics of the solute concentration at particular times and locations. The spatial moments of these plumes are random time series which have their own ensemble properties (Dagan, 1990). We can say that the plume ensemble is 'weakly ergodic' if the time-averaged derivatives of the first and second spatial moments of any replicate approach the corresponding ensemble mean quantities at large times (Papoulis, 1984). When this form of ergodicity applies the asymptotic (large time) ensemble mean plume will have the same overall size and shape as each replicate, although the smaller-scale details will generally differ. In practice it is important to know just how long it will take for a real plume to reach this asymptotic state.

Under certain special conditions, the ensemble mean concentration of a non-reactive solute satisfies a classical advection–dispersion transport equation with a constant (effective) velocity and macrodispersivity tensor. These effective properties may be derived from the velocity statistics which define the plume ensemble. If the ensemble is weakly ergodic the mean concentration obtained from the transport equation should have the same asymptotic first and second spatial moments as individual plumes. It is in this sense that we can say that macrodispersivities account for the large-scale effects of unresolved small-scale variability.

Generally speaking, the ensemble-based mean concentrations derived in stochastic transport theories provide good asymptotic approximations to individual plumes when the mean velocity is constant and the length scales of velocity fluctuations are small compared to the displacement and lateral dimensions of the plume. In such cases the plume has an opportunity to 'sample' a large range of velocity variations and is not unduly influenced by any particular anomaly. These are the somewhat idealized conditions that have applied in the field tests where macrodispersivities derived from stochastic theories have been most successful (McKay *et al.*, 1986; Freyberg *et al.*, 1986; Sudicky, 1986; Rajaram and Gelhar, 1991; Hess *et al.*, 1992). Ergodicity in field settings is usually checked by noting that the time

derivatives of the spatial moments of the field plume approach constant asymptotic values which are close to the corresponding moments of the derived ensemble mean. These requirements are generally satisfied in the experiments cited above, over times ranging from a few months to a few years.

Relatively few investigators have considered how macrodispersivity concepts focused on the effects of small-scale variability might be applied in more complicated field situations where large-scale variability is also important. Large-scale velocity variations reflect the effects of hydrogeologic features such as aquifer boundaries, stratigraphic sequences, depositional gradients, faults, surface water bodies, and regional or seasonal variations in recharge. Such features are typically represented deterministically in large-scale flow models. Most stochastic theories implicitly assume that a macrodispersivity tensor that works well when there is only small-scale velocity variability will also work well when there is larger-scale variability. This hypothesis has not been adequately verified in field settings. If the transformation from velocity to concentration were linear the effects of small and large-scale variability could be superimposed. But this transformation is nonlinear and velocity fluctuations at different scales may interact, in a process similar to modulation. It is difficult to say how important this effect might be without investigating particular cases.

In this paper we examine the applicability of classical macrodispersion concepts to situations where small and large-scale velocity variations are both present. It is important to emphasize that the two scales considered here do not represent the scales of actual geological features. Rather, the large scale represents resolved velocity variations (advective velocities specified explicitly in a numerical model) and the small scale represents unresolved velocity variations (velocities accounted for with a Fickian macrodispersivity coefficient). This approach enables us to conveniently partition the effects of multi-scale geological variability into two categories. The dividing line between large and small-scale variability depends on the data available for defining the advective velocity field and on the size of the grid cells used to model solute transport.

Our analysis relies on individual velocity and concentration realizations, as would occur in a field experiment. However these replicates are generated numerically, so they can be readily manipulated. In particular, we are able to simulate transport through velocity fields with only small-scale variability, only large-scale variability, or two-scales of variability (one small and one large). Although our analysis is performed without reference to particular stochastic theories, we recognize that our results have implications for the practical application of such theories. We comment on this in the final section of the paper.

There is a growing literature on alternative methods for characterizing multi-scale hydrogeologic variability and its effects on solute transport. In stochastic studies small-scale Eulerian velocity variations are most often modeled as time-invariant spatially-correlated random deviations from a constant mean. These velocity variations are generally assumed to be caused by small-scale hydraulic con-

ductivity fluctuations. Characteristic correlation lengths for small-scale hydraulic conductivity and velocity fluctuations are on the order of a few meters in the horizontal and a few centimeters in the vertical. In this paper we also treat small-scale velocity fluctuations as time-invariant correlated homogeneous random fields.

Most theoretical analyses of solute macrodispersion do not explicitly distinguish large-scale advective velocity fluctuations from smaller-scale dispersive fluctuations. The primary exceptions are a few studies which account for systematic (e.g. linear) log conductivity trends (Rubin and Seong, 1994; Indelman and Rubin, 1996). The large-scale effects of interest in our study are more complex and less systematic than such trends. This complexity could be captured if we obtained the large-scale velocity field from a typical deterministic regional flow simulation which includes irregular boundaries, variable soil properties and recharge rates, etc. Although such an approach has merit, it produces non-stationary fields which do not have well-defined velocity length scales or correlation structures. Here we adopt a different approach which is more compatible with the general philosophy of stochastic transport theory. Our large-scale velocity variations are also modeled as random time-invariant fluctuations about a constant mean but with much larger correlation lengths than the small-scale fields (Rajaram and McLaughlin, 1990). Typical correlation lengths for the large-scale features of interest here are on the order of tens of meters or more in the horizontal and meters in the vertical. Although the large-scale velocity fluctuations used in our experiment are generated randomly, they are assumed to be known perfectly. In this sense they represent the spatially variable but resolved portion of the velocity field that is included in the advective term of a traditional transport model.

Our numerical approach allows us not only to isolate different components of the velocity field but also to simulate transport with only local dispersion or with both local and macroscopic dispersion. These various options can be examined at much higher resolution and for much longer times and travel distances than is possible in a field experiment. Aggregate transport measures such as spatial moments or the peak concentration can be computed accurately and sensitivity analyses can be performed. Finally, extraneous factors such as temporal variations in the mean velocity can be avoided.

Of course, the results of our experiment are dependent on the assumptions and approximations we make. Since it is limited in fundamental ways this experiment does not provide a definitive assessment of the applicability of macrodispersion theory. However, the experimental results raise a number of questions which deserve further investigation. These are examined at the end of the paper.

2. The Computational Experiment

2.1. EXPERIMENTAL SETUP

Our computational experiment is intended to simulate a typical field tracer test, with solute released from an instantaneous point source into a steady flow field. We intentionally consider a single realization, rather than an ensemble, since our goal is to examine the applicability of macrodispersion concepts to field situations, rather than to confirm the ability of any particular theory to predict ensemble properties.

In order to be credible our experiment must be able to properly simulate small-scale velocity and concentration variability without introducing spurious oscillations or numerical dispersion. These are challenging requirements which can only be met with an accurate transport solver discretized on a high resolution spatial grid. Numerical accuracy comes at the cost of increased computational effort, leading to some difficult tradeoffs. For a given effort, we can choose between simulating three-dimensional transport in a relatively small spatial domain or simulating two-dimensional transport in a much larger domain. In this context, computational effort is related primarily to the number of spatial grid nodes and domain size is measured by the number of large correlation distances traveled. Also, we can choose between generating exact velocity fields from a computationally demanding flow simulator run over a small domain versus generating approximate velocity fields from a much more efficient random field generator run over a larger domain. These choices affect the types of questions we can examine as well as the generality of the results we can produce.

In this study we have given first priority to simulating transport over a large enough distance to allow the solute plume to adequately sample both the smallest and largest scales of velocity variability. As a result, we use a large two-dimensional (horizontal plane or plan view) domain with velocities obtained from a random field generator. The hydraulic conductivity in this domain is assumed to be isotropic and spatially variable. The domain extends over 200 large correlation lengths (λ_I) in the longitudinal (mean flow) direction and 12.5 large correlation lengths in the transverse direction. The left and right halves of the domain are illustrated in the upper and lower sections of Figure 1, respectively. We will examine detailed 'snapshots' of solute plumes located in the four windows indicated at time steps 10, 60, 100, and 300 (200, 1200, 2000, and 6000 days, respectively) after the instantaneous source release. These windows are defined for display purposes only – the domain used to solve the transport equation at all times is the $200\lambda_I$ by $12.5\lambda_I$ outer region shown in the figure. The release is distributed over the 20 m by 20 m square source area indicated in the figure and the mean flow is from left to right along the longitudinal (x_1) axis.

The random velocity generator used in our experiment relies on approximate velocity spectra derived from a specified log hydraulic conductivity spectrum and linearizations of Darcy's law and the groundwater flow equation (Ruan and McLaughlin, 1998). This approach is much less computationally demanding than currently

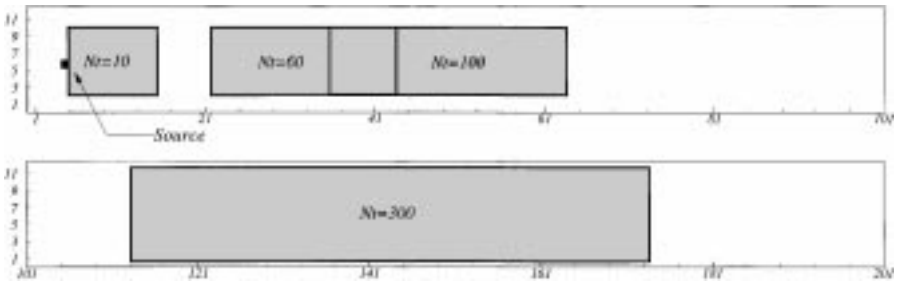

Figure 1. Left and right halves of experimental domain. Axes units in number of large log hydraulic conductivity correlation scales ($\lambda_l = 20$ m). Shaded areas indicate windows used to display results at time steps 10, 60, 100, and 300 (200, 1200, 2000, and 6000 days, respectively).

available methods for solving the groundwater flow equation with random coefficients on grids of order 10^6. Both theoretical and numerical analyses show that our linearized spectral approach provides physically reasonable divergence-free longitudinal and transverse velocities at each grid location (Graham and McLaughlin, 1988; Ruan and McLaughlin, 1998). In the simulations considered here we assume that the small and large-scale log conductivities are independent random fields, with Gaussian spectra characterized by correlation lengths λ_s and λ_l, respectively. We chose Gaussian spectra because they produce replicates with reasonably well-defined features that have length scales similar to the specified values of λ_s and λ_l.

The small and large-scale log conductivity spectra are used to derive the spectra of the corresponding linearized small and large-scale velocity fields. There is no need to actually generate random log conductivity replicates since the transport model only depends on velocity. We obtain a two-scale velocity field by summing the deviations of the small and large-scale velocity fields from their means

$$v_{it}(\mathbf{x}) = \overline{v_i} + v'_{is}(\mathbf{x}) + v'_{il}(\mathbf{x}), \tag{1}$$

where v_{it} is the two-scale velocity in direction i, v'_{is}, and v'_{il} are zero-mean small and large-scale velocity fluctuations in direction i, and $\overline{v_i}$ is the constant mean velocity in direction i. Figure 2 shows some typical longitudinal velocity realizations produced by our random field generator. The upper, middle, and lower plots are small-scale only, large-scale only, and two-scale realizations, respectively. These plots cover a small portion of our experimental domain extending over about 25 by 12.5 large correlation scales. The small-scale log conductivity correlation length is 2 m and the large-scale correlation length is 20 m, giving a scale disparity ratio of 1:10. Other inputs are summarized in Table I. Note that the longitudinal velocities are anisotropic, with longer correlation scales in the longitudinal (mean flow) direction. Also, note how the major features in the large-scale velocity field influence the two-scale field.

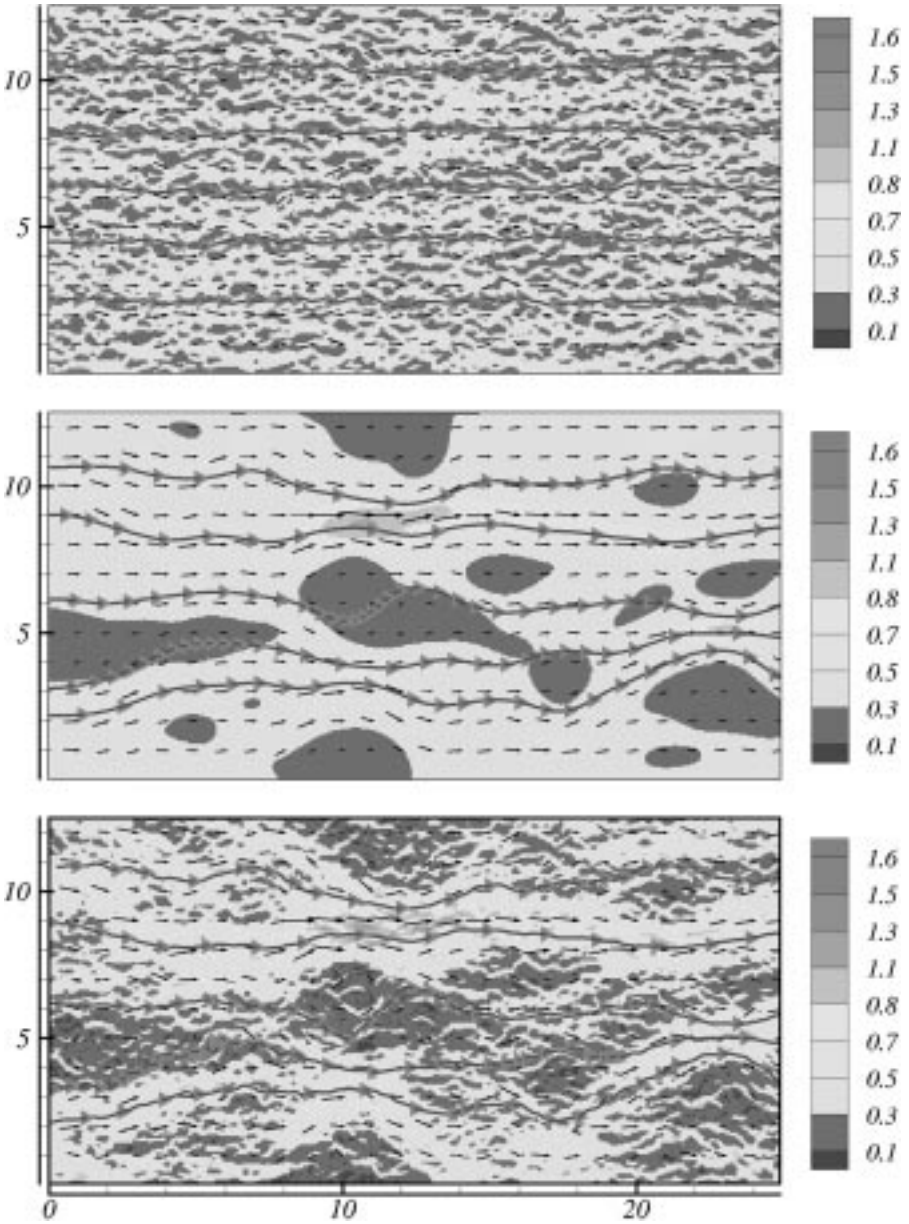

Figure 2. Synthetic realizations of longitudinal velocity for small ($\lambda_s = 2$ m), large ($\lambda_l = 20$ m) and two-scale log hydraulic conductivity spectra. Axis units in numbers of large correlation scales. Velocities are in m/day.

Table I. Input parameters for computational experiment

Domain size $L_1 \times L_2$	4080 m × 250 m
Grid size $\Delta x = \Delta x_1 = \Delta x_2$	1.0 m
Number of computational nodes N	1,024,331
Time step Δt	20 days
Total simulation time	8000 days (400 time steps)
Small-scale log hydraulic conductivity correlation length λ_s	2.0 m
Large-scale log hydraulic conductivity correlation length λ_l	20.0 m
Hydraulic conductivity geometric mean K_g	6.25 m/day
Log k variance σ_f^2	1.0
Porosity ρ	0.3
Mean hydraulic gradient $\|J\|$	0.02
Mean velocity $\overline{v}$	0.42 m/day
Local longitudinal dispersivity α_l	0.15 m
Local transverse dispersivity α_t	0.015 m
Longitudinal grid Peclet number	6.7
Transverse grid Peclet number	67.0
Courant number	8.2
Rectangular source size	20 m × 20 m
Source location (x_0, y_0)	(102 m, 125 m)

The solute transport equation which forms the basis for our numerical experiment can be written in generic form as

$$\frac{\partial c}{\partial t} + v_1 \frac{\partial c}{\partial x_1} + v_2 \frac{\partial c}{\partial x_2} = \frac{\partial}{\partial x_1}\left[D_{11}\frac{\partial c}{\partial x_1}\right] + \frac{\partial}{\partial x_2}\left[D_{22}\frac{\partial c}{\partial x_2}\right], \tag{2}$$

where t is time, $c(\mathbf{x}, t)$ is solute concentration, $v_1(\mathbf{x})$ and $v_2(\mathbf{x})$ are the spatially variable steady-state velocity components (small, large, or two-scale) in the longitudinal (x_1) and transverse (x_2) directions, and D_{11} and D_{22} are the longitudinal and transverse dispersion coefficients, aligned along the x_1 and x_2 directions, respectively. The dispersion coefficients are related to the dispersivities by

$$D_{11} = \overline{v}A_L, \qquad D_{22} = \overline{v}A_T, \qquad D_{12} = D_{21} = 0, \tag{3}$$

where A_{L} and A_{T} are, respectively, the longitudinal and transverse dispersivities.

We solve (2) with the cubic spline Eulerian–Lagrangian algorithm described in Ruan and McLaughlin (1999). This solver is computationally efficient and introduces little or no numerical dispersion at the grid resolutions we have used. Ruan and McLaughlin (1999), present a set of detailed quantitative tests of the cubic spline algorithm which demonstrate that it performs well in heterogeneous advection-dominated transport problems similar to the one considered here. When

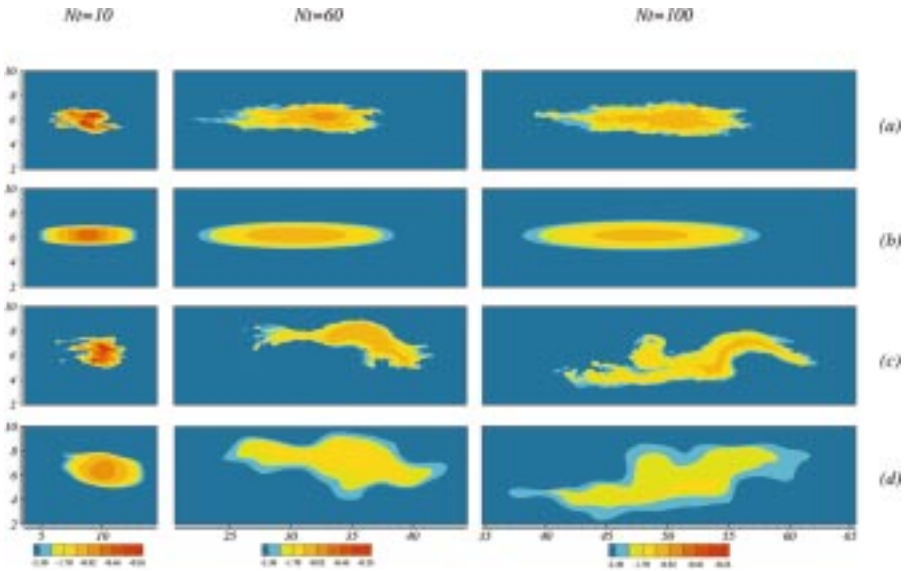

Figure 3. Solute log concentration contours at time steps 10 (left column), 60 (center column), and 100 (right column), corresponding to days 200, 1200, and 2000, respectively. First row (a) shows small-scale experimental plume (small-scale velocity with local dispersivity), second row (b) shows predicted (ensemble mean) small-scale plume (constant velocity with estimated macrodispersivity), third row (c) shows two-scale experimental plume (two-scale velocity with local dispersivity) and fourth row (d) shows predicted two-scale plume (large-scale velocity with estimated macrodispersivity). Compare (b) to (a) and (d) to (c).

compared to traditional Eulerian or Eulerian–Lagrangian methods, the cubic spline interpolator yields smaller computational errors for a given level of computational effort while allowing the use of larger Courant and Peclet numbers. The accuracy of the cubic spline transport solver is also demonstrated by its ability to resolve small-scale highly variable plume features without adding spurious oscillations (see Figures 3c and 4c).

In our experiment the concentration is specified to be zero on the left boundary of the computational domain. Outflow conditions are specified on the remaining boundaries. The outflow conditions allow streamlines to cross boundaries. They are implemented in the dispersive step of our Eulerian–Lagrangian solution algorithm by fixing the outflow boundary concentration at the value obtained from the preceding advective step (see Ruan and McLaughlin (1999) for details). The initial concentration is zero everywhere in the computational domain, except over the source region, where it is equal to the specified source concentration c_s.

2.2. INVESTIGATION OF MACRODISPERSIVE TRANSPORT

We now wish to use our experimental setup to examine the performance of a transport model which uses macrodispersivities to account for the effects of small-

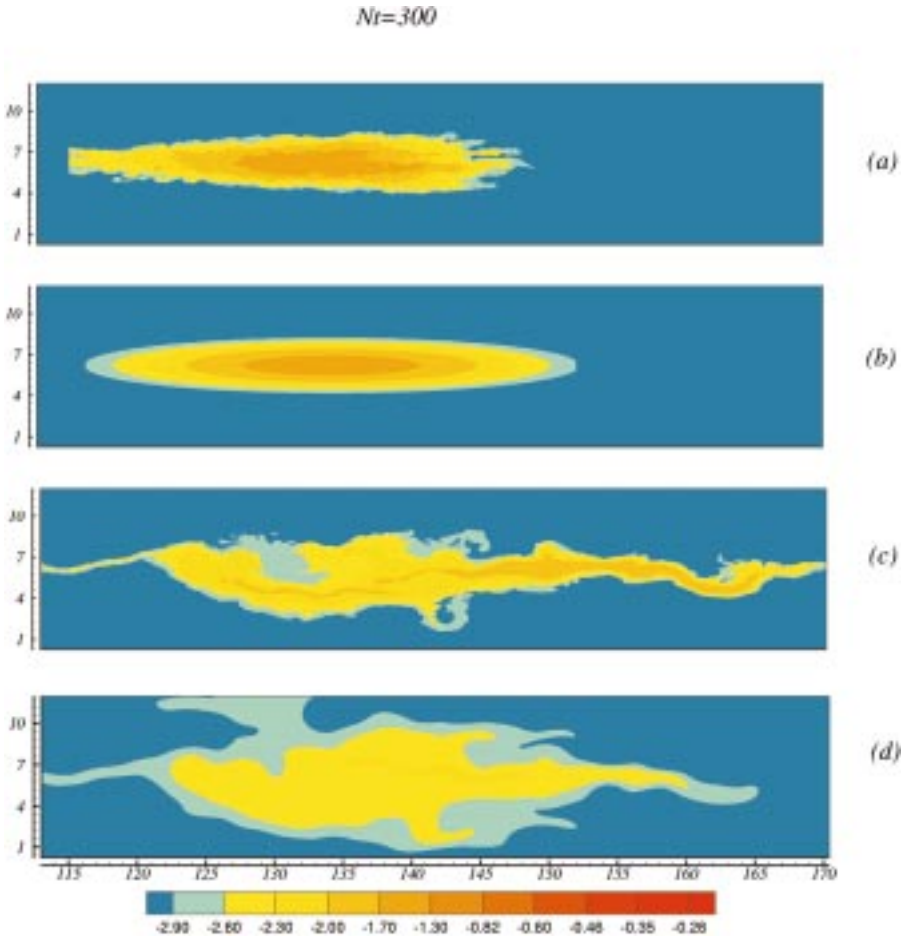

Figure 4. Solute log concentration contours at time steps 300, corresponding to day 6000. Rows are defined as in Figure 3.

scale variability. This raises the question of how we should compute the macrodispersivity tensor. If we use theoretically derived macrodispersivity values we introduce the possibility of inconsistencies between approximations made in the numerical experiment and approximations made in the theory. For example, the two-dimensional asymptotic macrodispersivities of Gelhar and Axness (1983) are based on linearizations of both the flow and transport equations while our experiment relies on a linearization of the flow equation (since the velocity random field generator is based on a linearization) but retains all the nonlinearities introduced by the transport process.

In order to avoid such inconsistencies, we adopt a different approach. The constant velocity and macrodispersivity used in the ensemble mean transport equation are related to the asymptotic spatial moments of the mean concentration (the velocity is the time derivative of the first moment while the macrodispersivity is

proportional to the time derivative of the second moment). If the assumptions of the stochastic theories are correct, the weak ergodicity assumption should hold and the asymptotic spatial moments of the smooth ensemble mean plume should be essentially the same as the asymptotic moments of the irregular experimental plume. Consequently, we can estimate the desired constant velocity and macrodispersivity from the spatial moments of the experimental plume. The latter alternative is analogous to estimating effective transport properties from a tracer test in a domain where there is only small-scale variability. It has the advantage of focusing on the common objective of most of the stochastic theories without depending on the assumptions of any particular theory.

We begin by generating an experimental plume that emanates from an instantaneous point source and moves through a velocity field with only small-scale variability about a constant mean. These are the conditions considered in classical macrodispersion theory. The first rows (Case a) of Figures 3 and 4 show log concentration contour plots obtained at four different times for such a plume. Table II summarizes the velocity and dispersivity assumptions made for this and all of the other cases simulated in our experiment.

Note that only local dispersivity is used in the (Case a) simulation since small-scale velocity fluctuations are explicitly included in the advective term of the transport equation. The resulting tracer plume has a roughly Gaussian shape, with quite a bit of fine structure contributed by small-scale velocity variations. The very presence of this fine structure is a qualitative indication of the cubic spline algorithm's ability to solve difficult advection-dominated transport problems. Even a small amount of numerical dispersion tends to suppress such features.

The first and second moments of an ensemble mean plume are related to the constant effective velocity and macrodispersivity in the solute transport equations

Table II. Summary of experimental cases

Case	v_1	v_2	A	Comments
(a)	$\overline{v} + v_{s1}$	v_{s2}	Local only	Small-scale experimental plume, no large-scale variability
(b)	$\overline{v}$	0	Local + macrodispersivity	Predicted (ensemble mean) small-scale plume, small-scale variability not resolved but accounted for with macrodispersivity, no large-scale variability
(c)	$\overline{v} + v_{t1}$	v_{t2}	Local only	Two-scale experimental plume, both small and large-scale variability
(d)	$\overline{v} + v_{l1}$	v_{l2}	Local + macrodispersivity	Predicted two-scale plume, small-scale variability not resolved but accounted for with macrodispersivity, large-scale variability resolved

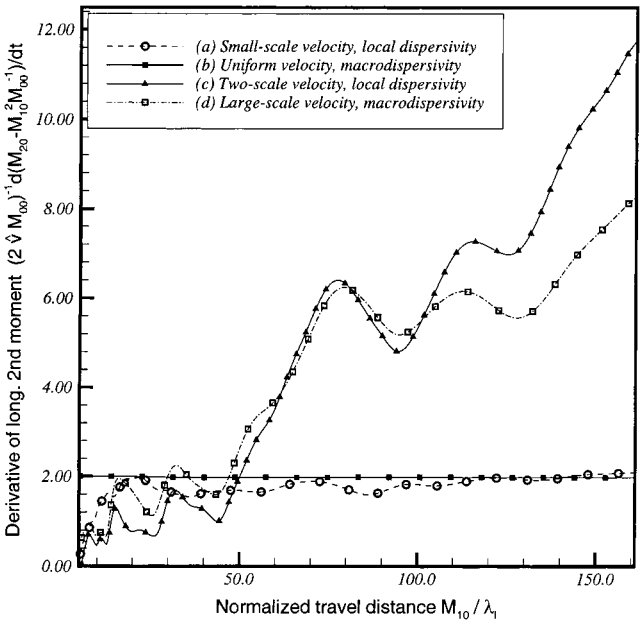

Figure 5. Normalized time derivative of longitudinal second spatial moment $(2\widehat{v}M_{00})^{1/2}d \cdot (M_{20} - M_{10}^2 M_{00}^{-1})/\mathrm{d}t$ versus normalized travel distance (M_{10}/λ_I) for each of the cases shown in Figures 3 and 4.

as follows (Dagan, 1989; Gelhar; 1993):

$$\widehat{v} = \frac{1}{M_{00}} \frac{\mathrm{d}M_{10}}{\mathrm{d}t}, \tag{4}$$

$$\widehat{A}_{\mathrm{L}} = \frac{1}{(2\hat{v}M_{00})} \frac{\mathrm{d}(M_{20} - M_{10}^2 M_{00}^{-1})}{\mathrm{d}t}, \tag{5}$$

$$\widehat{A}_{\mathrm{T}} = \frac{1}{(2\hat{v}M_{00})} \frac{\mathrm{d}(M_{02} - M_{01}^2 M_{00}^{-1})}{\mathrm{d}t}, \tag{6}$$

where M_{ij} is the (i, j)th spatial moment, defined in discrete form as

$$M_{ij}(t) = \sum_{k=1}^{N} x_{k1}^i x_{k2}^j \, c(x_{k1}, x_{k2}, t) \, \Delta x \Delta x \tag{7}$$

and $M_{00}(t)$ is the solute mass (practically a constant for our simulations). If we substitute the nodal concentrations from the small-scale experimental plume into (7) we find that the time derivatives on the right-hand sides of (4) through (6) vary over time. The first moment time derivative fluctuates slightly about the ensemble mean velocity of 0.42 m/day used in the random field generator. Figures 5 and 6 reveal that the longitudinal and transverse central second moment time derivatives

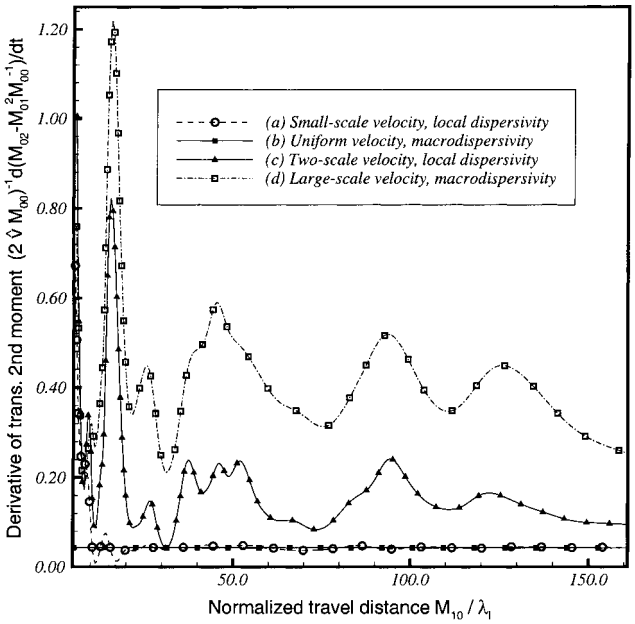

Figure 6. Normalized time derivative of transverse second spatial moment $(2\hat{v}M_{00})^{1/2}d \cdot (M_{02} - M_{01}^2 M_{00}^{-1})/\mathrm{d}t$ versus normalized travel distance (M_{10}/λ_l) for each of the cases shown in Figures 3 and 4.

for Case a (small circles) fluctuate initially but soon approach constant asymptotic values, a prerequisite for ergodicity. We substitute these asymptotic values into (4) through (6) to obtain the effective velocity and macrodispersivity for our ensemble mean model. Note that this forces the ergodicity condition to apply.

If we insert the asymptotic effective velocity and macrodispersivities derived from Case a into the solute transport Equation (2) the result is the predicted (ensemble mean) small-scale plume shown in the second rows of Figures 3 and 4 (Case b). As expected, the Case b plume has a Gaussian shape with the same asymptotic first and second spatial moments as the Case a plume in Figures 3(a) and 4(a). This is confirmed by the Case b second moment time derivatives plotted in Figures 5 and 6 (small filled squares).

Although the predicted plume of Figures 3(b) and 4(b) has the same first two spatial moments as the more irregular plume in Figures 3(a) and 4(a), the smaller-scale differences between these two cases are apparent. Most striking is the moderate longitudinal asymmetry (non-zero third moment) of the irregular plume. Despite minor differences between Cases a and b, it might be argued that the predicted plume provides a reasonable aggregate approximation to the irregular plume. This prediction does not resolve small-scale variations in velocity but, instead, uses a macrodispersivity coefficient to account for their aggregate effect.

Other quantitative measures of plume structure provide additional insight which can help us compare our experimental cases. One of these is a dilution (or entropy)

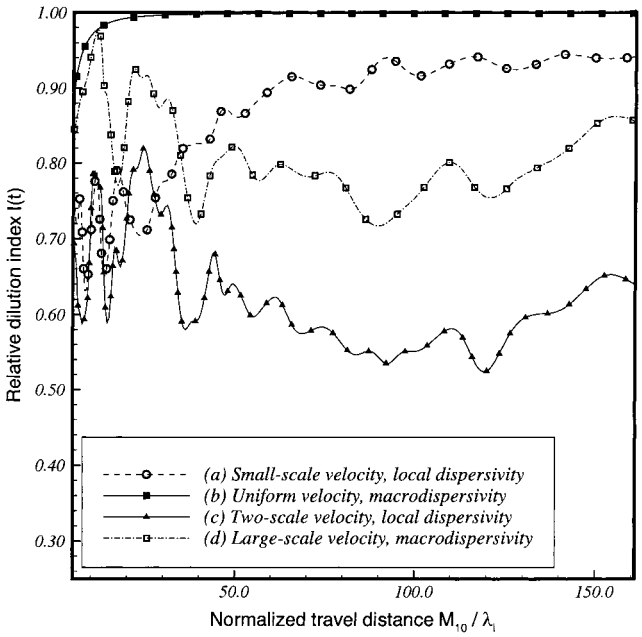

Figure 7. Relative dilution index ($I(t)$) versus normalized travel distance (M_{10}/λ_l) for each of the cases shown in Figures 3 and 4.

index based on concepts proposed by Kitanidis (1994). This index is defined as

$$I(t) = E(t)/E_{\max}(t), \tag{8}$$

where

$$E(t) = \exp\left\{-\sum_{k=1}^{N} p_k \log p_k \Delta x \Delta x\right\} \tag{9}$$

and $E_{\max}(t)$ is the maximum value of $E(t)$. The ratio $p_k(t) = c_k(t)/M_{00}(t)$ is the normalized solute concentration at time t and node k. Figure 7 plots the dilution index versus normalized travel distance for each of our experimental cases.

It can be shown that the value $E_{\max}(t)$ is attained when $c_k(t)$ corresponds to a Gaussian plume with the same second spatial moments as the plume of interest (Kitanidis, 1994). That is, the Gaussian condition is the one that provides the most dilution or mixing. The dilution index $I(t)$ measures the ratio of area (or volume) occupied by a simulated plume to the area (or volume) occupied by the corresponding Gaussian plume. When $I(t)$ approaches 1.0 the plume is as well-mixed as possible, for a given set of spatial second moment values. This interpretation is confirmed by noting that the dilution index for Case b approaches the maximum value of 1.0 as soon as velocity variations overcome the initialization effects imposed by the square solute source. Although the dilution index for Case a does not

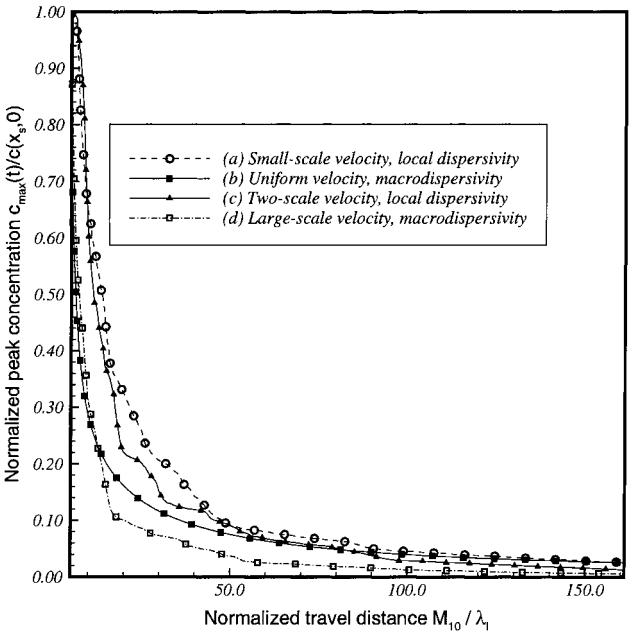

Figure 8. Normalized peak solute concentration $c_{\max}(t)/c_s$ versus normalized travel distance (M_{10}/λ_l) for each of the cases shown in Figures 3 and 4.

reach 1.0 it approaches an asymptotic value above 0.90, indicating that this case produces a nearly Gaussian plume.

Another important measure of plume behavior is the maximum (or peak) concentration taken over all simulation nodes. Figure 8 plots the normalized peak concentration $c_{\max}(t)/c_s$ versus normalized travel distance for each of our experimental cases. Here c_s is the initial source concentration. Note that the normalized peak decays quickly from its maximum value of 1.0 for both Cases a and b. However, the peak for Case a, which retains small-scale variability, is consistently higher than the peak for Case b, which accounts for small-scale variability only through the enhanced spreading provided by the macrodispersivity coefficients. The differences in the two peaks are greatest at intermediate times when the peak values are moderately large. At these times the peaks for Case a can be twice the values obtained for Case b.

Figure 9 provides a more global indication of the distribution of simulated concentration values. The measure plotted here is a cumulative areal distribution function of the concentration at four times after the initial solute release. At each of these times concentrations at all computational nodes with values greater than the threshold $10^{-6}c_{\max}(t)$ are ranked from smallest to largest ($c_{\max}(t)$ is the maximum concentration over all nodes at time t). This rank is then divided by the number of nodes N_{cmax} which have concentrations above the threshold to give a number between 0.0 and 1.0. The normalized rank and concentration are plotted for each

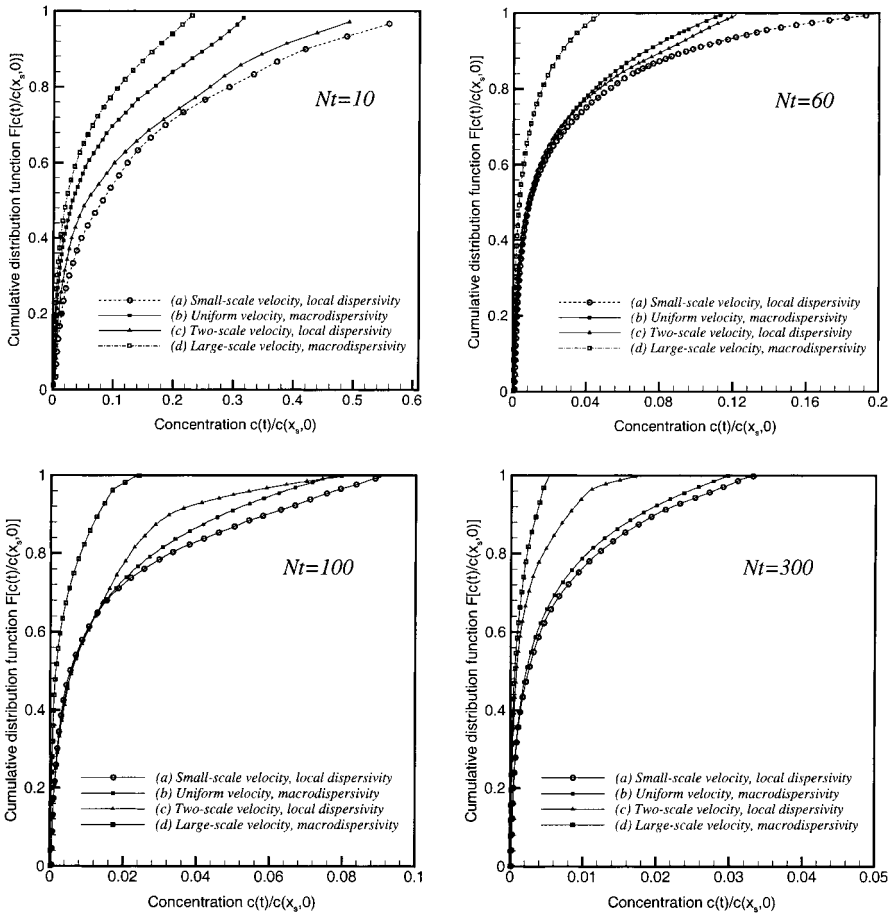

Figure 9. Cumulative areal distribution functions $F(c)$ of solute concentration versus normalized concentration for each of the cases shown in Figures 3 and 4.

of the N_{cmax} nodes, giving the curves shown in Figure 9. Since every node has an associated area Δx^2 the ordinate of each curve can be viewed as the fraction of the plume area with concentrations less than or equal to the value specified on the abscissa. It is apparent from the plot that the concentrations obtained for Case a are consistently higher than those obtained for Case b at early times but nearly the same at later times. This appears to reflect the time needed in Case a for local dispersion and small-scale velocity fluctuations to dilute the solute originally concentrated at the source.

The results discussed above for Cases a and b confirm the basic assumptions of stochastic macrodispersion theory, particularly the rapid convergence of the spatial moment time derivatives to asymptotic values and the near-Gaussian appearance of the asymptotic plume. This supports the use of macrodispersivities in situations

where velocity varies only over small scales. Now we can examine the results obtained when large-scale velocity variations are also present.

The third rows (Case c) of Figures 3 and 4 show the evolution of an experimental solute plume through a two-scale velocity field with only local dispersion included. Case c is analogous to Case a except for the addition of a large-scale velocity component. We can consider this to be a more-or-less realistic case which we would like to reproduce, at least in an aggregate fashion, with a model based on effective properties. The Case c plume clearly has a less regular structure than Cases a and b, reflecting the influence of large-scale flow features. This is most apparent at time step $N_t = 100$, when cross-sections through portions of the plume are multi-modal and the area of highest concentration runs nearly perpendicular to the mean flow direction.

Some of the quantitative measures used to analyze Cases a and b behave much differently for Case c. Figure 5 indicates that the time derivative of the longitudinal spatial second moment (small triangles) does not approach an asymptotic value even after the plume has traveled 150 large correlation lengths (1500 small correlation lengths). This means that the weak ergodicity condition cannot be satisfied, at least over the time period considered in this experiment. Although the transverse component plotted in Figure 6 does vary around a constant value after about 50 large correlation scales this value is significantly larger than the ones obtained for Cases a and b.

Figure 7 shows that the Case c dilution index is much lower than the indices obtained for Cases a and b, confirming the visual observation that the two-scale plume is not Gaussian and not as well mixed as plumes which have a more Gaussian shape. The peak concentration measure of Figure 8 indicates that the Case c plume has lower peak values than Case a except at very early times. This may reflect the marked stretching of the two-scale plume that takes place starting after time step $N_t = 60$. The cumulative areal distribution functions plotted in Figure 9 confirm that Case c has consistently lower concentrations than Case a with the difference increasing over time.

Now we can consider what happens when we insert the effective dispersivities estimated from Case a into a transport equation which resolves the large-scale features of the Case c flow field. In particular, we are interested in the ability of these macrodispersivities to account for the effects of small-scale variability. The resulting plume, which can be viewed as a prediction of Case c, is shown in the fourth rows of Figures 3 and 4 (Case d)). The Case d plume reproduces the general location and shape of the Case c plume, although it is much smoother. The most noticeable qualitative difference is at the higher concentration levels, especially at later times. At $N_t = 100$ the Case c peak is higher and in a different location than the Case d peak and the region of moderately high concentrations is more extensive in Case c. The contrast is much more pronounced at $N_t = 300$, when the predicted plume has nearly disappeared and the concentrations levels along its centerline are greatly underestimated.

Table III. Summary of mass balance errors (in percent)

Case	(a)	(b)	(c)	(d)
$N_t = 10$	−3.28	−0.18	−0.80	−0.25
$N_t = 60$	−5.74	0.25	−1.36	−0.02
$N_t = 100$	−4.03	0.46	0.23	0.89
$N_t = 300$	−4.85	1.02	3.40	14.66

Additional insight can be obtained by comparing the Case c and d quantitative measures plotted in Figures 5 through 9. The longitudinal second moment time derivatives for Cases c and d are quite similar up to about 100 large correlation distances (time step $N_t = 100$). After that, the Case d time derivative increases more slowly, underestimating the longitudinal spreading of the Case c plume. The transverse second moment time derivative of the predicted plume (open squares) is significantly larger than the comparable Case c result at large times. This indicates that the Case d plume is spreading more rapidly in the transverse direction, as is apparent in Figures 3 and 4. Many of these differences between the Case c and d second moment plots are probably replicate-specific. The more general phenomenon noted here is the lack of convergence to asymptotic values, especially in the longitudinal direction, even after 150 large-scale correlation distances. This indicates that a critical prerequisite for ergodicity (moment derivative convergence) is not satisfied.

The dilution index plotted in Figure 7 indicates that the predicted Case d plume is much better mixed and 'more Gaussian' than the Case c plume, reflecting the smoothing effect of the macrodispersivity. Figures 8 and 9 confirm that this effect lowers the peak concentration and shifts the cumulative areal distribution function towards lower values at all times. Overall, the effective property approximation locates the solute reasonably well but consistently underestimates its concentration. This could have serious implications for applications where concentration levels are important, either for regulatory reasons or because of possible effects on chemical and biological transformations not considered here.

Since the plumes in Figures 3 and 4 are plotted with discrete log concentration intervals (one color for each interval) it is difficult to visually confirm that their masses are all the same. Table III summarizes computed mass balance errors (initial mass released at the source minus plume mass at the specified time) for each of the four cases shown in Figures 3 and 4. All the errors are small (a few percent or less) except the error for Case d at time $N_t = 300$. In this case the plume spread so much that some of it (about 15% of the initial mass) crossed the outflow boundary and left the computational domain. Some of the other plumes shown in Figures 3 and 4 extended slightly outside the viewing windows defined in Figure 1 and so appear to be truncated. However, the mass balance results show that only the Case d $N_t = 300$ plume actually spread outside the computational domain.

It is interesting to note that Figure 9 indicates that the Case c solute concentrations are close to Case a but much higher than Case d at early times. As time progresses the Case c concentrations become smaller relative to Case a until they approach the values of Case d. This evolutionary process suggests that the two-scale plume is first influenced primarily by the smaller-scale velocity variations which also control the dispersion and dilution of the Case a plume. As larger-scale features take effect, they appear to contribute additional mixing which lowers concentrations well below the levels observed in the small-scale plume. The moments for Case c suggest that this large-scale mixing effect may have a different form than classical Fickian macrodispersion but it does, nevertheless, disperse and dilute the solute. It is possible that the large-scale mixing effect may be described as Fickian macrodispersion over larger time scales than considered here, but it should be noted that our two-scale plume has traveled well over 100 large correlation scales without reaching this state. Even if the plume eventually reaches a asymptotic Fickian (i.e. Gaussian) state, this will occur after the solute has become very dilute, with concentrations orders of magnitude below the source value. Asymptotic Fickian models which apply only at such large times are of limited practical usefulness.

3. Discussion and Conclusions

The numerical experiment described here, like a field tracer experiment, provides information about solute movement for particular conditions. If these conditions change we can expect the resulting plumes to change as well. In particular, plumes obtained from different velocity replicates can be expected to have features which differ qualitatively from those shown in Figures 3 and 4. Although some care must be exercised in generalizing from the results reported here, we have repeated our experiment with different replicates and have observed similar overall behavior. Furthermore, we believe that the plumes discussed in this paper have traveled sufficiently far to sample a wide range of velocity fluctuations, both at the small and large scales. So we feel that it is valid to draw some general conclusions from our results.

We have observed (for Case a) that the time derivatives of the spatial moments of an individual solute plume moving through a small-scale constant mean velocity field tend to asymptotic limits. Furthermore, this plume approaches the well-mixed Gaussian state associated with a relative dilution index of 1.0. Since Gaussian plumes are completely characterized by their first two spatial moments we might expect that a model which reproduces these asymptotic moments will provide good predictions in other respects, at least for large times.

We have investigated this hypothesis with a transport model which does not resolve small-scale velocity fluctuations but is able to reproduce the spatial moments of the small scale plume with an appropriately adjusted macrodispersion coefficient. Predictions from the model (Case b) match the overall shape of the small-scale plume and give reasonable approximations to the large-time dilution

index, peak value, and cumulative areal distribution function. So the first part of our experiment confirms that the most of the effects of small-scale velocity variability can be accounted for with a macrodispersion coefficient, at least for large times, if there is no large-scale variability.

The situation appears to change when small and large-scale velocity fluctuations are both present (Case c). The resulting plume is qualitatively different from the classical Gaussian plume since it reflects the cumulative influence of all the large-scale features it has passed through. The longitudinal second spatial moment time derivative does not converge to an asymptotic value, even after the plume has traveled over one hundred large correlation lengths and the peak concentration has dropped to less than 1–2% of the initial source concentration. The corresponding transverse derivative appears to approach an asymptotic value, but this value is significantly larger than the one observed for the small-scale plume of Case a. The dilution index confirms that the two-scale plume remains far from Gaussian throughout the simulation period. Although it might be argued that the plume should eventually become Gaussian it appears that this state could only be obtained after the concentrations have been diluted far below the small levels observed at the end of our experiment.

The primary question motivating our investigation is whether the large-scale features of a two-scale solute plume can be reproduced by a model which perfectly resolves the large-scale component of the velocity field but uses macrodispersivities to account for small-scale variability (Case d). As might be expected, the plume predicted by such a model shares some qualitative features with the two-scale experimental plume, since they both depend on the same large-scale velocity field. But the predicted plume is more well-mixed and consistently underestimates peak solute concentrations at all times. So it appears that a model which uses conventional macrodispersivities to account for small-scale variability fails to reproduce some key features (especially peak concentrations) of the two-scale plume. It may be argued that since an ensemble mean concentration model based on effective parameters is intended to produce a smoothed version of the actual plume the results shown in Figure 4(d) should come as no surprise. The problem with the prediction of Figure 4(d) is not that it is smooth but that it fails to reproduce either the first two spatial moments of the two-scale plume (the weak ergodicity requirement) or its peak values, which may be more important than the moments in practical applications.

It should be pointed out that the two-scale plume considered in our experiment may be too narrow (with respect to the length of large-scale velocity variations) to display ergodic behavior over the time scales we have simulated. This is, in fact, one of our primary points. If large-scale velocity variations are larger than source sizes, as they are in many practical modeling applications (where advective velocities may be defined over grid spacings on the order of hundreds of meters and sources may be only tens of meters across), we cannot expect ensemble mean dispersion theories to accurately predict the behavior of individual plumes. The

source sizes and large-scale velocity correlation lengths we have used are typical of many field situations. If the requirements needed for stochastic macrodispersion theories to hold are too confining these theories may be of limited practical use, even if they are correct for a particular set of assumptions. Non-Fickian and non-local theories of macrodispersion provide alternatives to the simple approach considered in Figure 4(d) (see, for example, Graham and McLaughlin, 1988). However, these theories generally replace traditional effective property concepts and associated transport equations with more complex alternatives. Also, they have not been extensively tested in field settings where large-scale velocity variations are important.

In many ways this experiment raises as many questions as it answers. How valid are conclusions drawn from a two-dimensional experiment which ignores the effects of mixing in the missing third dimension? How would the results differ if the velocity field were generated from a nonlinear flow simulator rather than a random field generator based on a linearizations of Darcy's law and the flow equation? Could a different macrodispersivity coefficient (e.g. one which accounts in some way for the presence of large-scale variability) do a better job in predicting dilution or concentration peaks? How about a non-local stochastic dispersion theory or one which treats the large-scale velocity component as a spatially variable ensemble mean? How would the situation change if the macrodispersivities were derived from statistics (e.g. velocity covariances) conditioned on the resolved large-scale velocity field, rather than from unconditional statistics? These are all questions which go beyond the scope of this paper but which deserve careful attention.

But the critical issue raised here is whether it is valid to assume that small and large-scale velocity fluctuations can be treated independently. We believe that the substantial difference in behavior observed for our two-scale case, even after travel over distances unprecedented in other field or numerical experiments, can best be explained by scale interactions resulting from the nonlinear transformation from velocity to concentration (Ruan, 1997). If this transformation were linear, our two-scale velocity field would be just one more statistically homogeneous (spatially stationary) input to classical macrodispersion theory. We would expect the spatial moment derivatives and dilution index to approach classical values, albeit more slowly than in the small-scale case. Since this does not appear to happen we suspect that scale interactions are important. This hypothesis is considered further in Ruan (1997), where a number of numerical sensitivity studies are described. However, the issue will probably be resolved only through more careful theoretical analysis of the nonlinear aspects of the transport process.

Acknowledgements

The authors wish to thank Prof. Wolfgang Kinzelbach, who offered many valuable suggestions and comments, and Prof. Lynn Gelhar, who provided helpful reviews of earlier versions of this work.

References

Adams, E. E. and Gelhar, L. W.: 1992, Field study of dispersion in a heterogeneous aquifer: spatial moments analysis, *Water Resour. Res.* **28**(12), 3293–3308.

Dagan, G.: 1984, Solute transport in heterogeneous porous formations, *J. Fluid Mech.* **145**, 813–833.

Dagan, G.: 1986: Statistical theory of groundwater flow and transport: pore to laboratory, laboratory to formation and formation to regional scale, *Water Resour. Res.* **22**(9), 120S–134S.

Dagan, G.: 1989, *Flow and Transport in Porous Formations*, Springer-Verlag, New York.

Dagan, G.: 1990, Transport in heterogeneous porous formations: spatial moments, ergodicity, and effective dispersion, *Water Resour. Res.* **26**(6), 1281–1290.

Freyberg, D. L.: 1986, A natural gradient experiment on solute transport in a sand aquifer, 2, Spatial moments and the advection and the dispersion of nonreactive tracers, *Water Resour. Res.* **22**(13), 2031–2046.

Gelhar, L. W. and Axness, G. L.: 1983, Three-dimensional stochastic analysis of macrodispersion in aquifers, *Water Resour. Res.* **19**(1), 161–180.

Gelhar, L. W.: 1986, Stochastic subsurface hydrology from theory to applications, *Water Resour. Res.* **22**(9), 135S–145S.

Gelhar, L. W.: 1993 *Stochastic Subsurface Hydrology*, Prentice Hall, Englewood Cliffs, New Jersey.

Hess, K. M., Wolf, S. H. and Celia, M. A.: 1992, Large-scale natural gradient tracer test in sand and gravel, Cape Cod, Massachusetts, 3, Hydraulic conductivity and calculated macrodispersivities, *Water Resour. Res.* **28**(8), 2011–2027.

Indelman, P. and Rubin, Y.: 1996, Solute transport in nonstationary velocity fields, *Water Resour. Res.* **32**(5), 1259–1267.

Kitanidis, P. K.: 1994, The concept of dilution index, *Water Resour. Res.* **30**(7), 2011–2026.

McKay, D. M., Freyberg, D. C., Roberts, P. V. and Cherry, J. A.: 1986, A natural gradient experiment on solute transport in a sand aquifer, 1, Approach an overview of plume movement, *Water Resour. Res.* **22**(13), 2017–2030.

Neuman, S. P., Winter, C. L. and Newman, C. M.: 1987, Stochastic theory of field-scale Fickian dispersion in anisotropic porous media, *Water Resour. Res.* **23**(3), 453–466.

Papoulis, A.: 1984, *Probability, Random Variables, and Stochastic Processes*, McGraw-Hill, New York, NY.

Rajaram, H. and McLaughlin, D.: 1990, Identification of large-scale spatial trends in hydrologic data, *Water Resour. Res.* **26**(10), 2411–2423.

Rajaram, H. and Gelhar, L. W.: 1991a, Three dimensional spatial moment analysis of the Borden tracer test, *Water Resour. Res.* **27**(6), 1239–1251.

Rehfeldt, K. R., Boggs, J. M. and Gelhar, L. W.: 1992, Field study of dispersion in heterogeneous aquifer, 3, Geostatistical analysis of hydraulic conductivity, *Water Resour. Res.* **28**(12), 3309–3324.

Ruan, F.: 1997, A numerical investigation of solute plumes in nested multi-scale porous media, PhD thesis, Mass. Instit. Tech., Cambridge, MA.

Ruan, F. and McLaughlin, D. B.: 1998, An efficient multivariate random field generator using the fast fourier transform, *Advances Water Resour.* **21**(5), 385–399.

Ruan, F. and McLaughlin, D. B.: 1999, An investigation of Eulerian–Lagrangian methods for solving heterogeneous advection-dominated transport problems, *Water Resour. Res.* (in press).

Rubin Y. and Seong, K.: 1986, Investigation of flow and transport in certain cases of nonstationary conductivity fields, *Water Resour. Res.* **30**(11), 2901–2911.

Sudicky, E. A.: 1986, A natural gradient experiment on solute transport in a sand aquifer: spatial variability of hydraulic conductivity and its role in the dispersion process, *Water Resour. Res.* **22**(13), 2069–2082.